Applied Catalysis B: Environmental 125 (2012) 358–366

Contents lists available at SciVerse ScienceDirect

Applied Catalysis B: Environmental

journal homepage: www.elsevier.com/locate/apcatb

Coverage of carbon nanotubes with titania nanoparticles for the preparation of active titania-based photocatalysts

Sakae Takenaka*, Takafumi Arike, Hideki Matsune, Masahiro Kishida

Department of Chemical Engineering, Graduate School of Engineering, Kyushu University, Moto-oka 744, Nishi-ku, Fukuoka 819-0395, Japan

ARTICLE INFO

Article history:
Received 1 May 2012
Received in revised form 5 June 2012
Accepted 12 June 2012
Available online 20 June 2012

Keywords:
Carbon nanotube
Titania
Titania-coated carbon nanotube
Pt metal
Photocatalyst

ABSTRACT

TiO_2 nanoparticles were deposited on carbon nanotubes (CNTs) to improve their photocatalytic activity. The outer surface of the CNTs could be uniformly covered with TiO_2 nanoparticles using the hydrolysis of titanium tetraisopropoxide ($Ti(O^iPr)_4$) in the presence of urea or glycine amide. The urea and glycine amide acted as linker molecules between the TiO_2 nanoparticles and the CNT surfaces. The TiO_2-coated CNTs showed a higher catalytic activity for the photodegradation of organic molecules than TiO_2 alone. The addition of the CNTs to the TiO_2 photocatalytic system retarded the recombination of the electron–hole pairs generated in the photo-irradiated TiO_2. When Pt metal particles were inserted in the cavities of the CNTs in the TiO_2-coated CNT catalyst system, further improvements in the photocatalytic activity were observed. The TiO_2-coated CNTs with Pt metal particles displayed a unique catalytic performance in the photocatalytic degradation of organic impurities in water.

1. Introduction

Carbon nanotubes (CNTs) have attracted much attention due to their specific structure-dependent physical, chemical and electronic properties. To optimize the use of CNTs in various applications, CNTs have been functionalized with other nanostructures such as polymers and metal or metal oxide nanoparticles [1]. The combination of the unique properties of CNTs opens the possibility of using CNTs for advanced applications, such as reinforcements in composite materials, or catalysts [2–5]. CNTs are excellent supports for photocatalysts, because of their chemical stability, high electron conductivity and high surface area [6,7]. TiO_2 is one of the most important photocatalysts because of its high durability, its relative non-toxicity and its chemical inertness and corrosion resistance. TiO_2 has been applied as a photocatalyst for the removal of organic contaminants in water or air and for the formation of hydrogen through water splitting [8–10]. Irradiation with UV light causes the photoactivation of TiO_2, leading to the generation of electron–hole pairs. The electron–hole pairs in TiO_2 have strong redox properties, which allow the catalysis of various reactions. However, the quantum yield of TiO_2 is not so high, due to the rapid recombination of the photogenerated electrons and holes. Therefore, TiO_2 is frequently combined with CNTs. The electrons generated by the photo-irradiation of the TiO_2 and CNTs composites are transferred from the TiO_2 to the CNTs, which retards the recombination of the photogenerated electrons and holes. The photocatalytic activity of TiO_2 is thus enhanced by its combination with CNTs. TiO_2–CNT composites have frequently been prepared using sol–gel methods with titanium alkoxides [11–13]. However, the deposition of TiO_2 onto CNT surfaces is a challenging task, due to the chemical inertness of CNTs. The introduction of functional groups such as —COOH and —OH onto CNTs enhances the interaction between CNTs and TiO_2 [14,15]. However, the density of TiO_2 nanoparticles deposited on CNT surfaces using these methods is not always high because of low density of functional groups on the CNT surfaces and/or weak interactions between the TiO_2 and the functional groups [16]. CNTs are sometimes modified with surfactant molecules such as sodium dodecylsulfate or polyethyleneimine [17–19]. The use of these surfactants leads to strong interactions between CNTs and the TiO_2 particles. However, it is difficult to remove the surfactant molecules from the CNTs without damaging the CNT surfaces; it is necessary to remove the surfactants because they sometimes spoil the photocatalytic activity of the TiO_2–CNT composites. Novel methods for the dense and uniform deposition of TiO_2 nanoparticles on CNT surfaces are therefore required.

When TiO_2–CNT composites are photo-irradiated, electron–hole pairs are generated in the TiO_2 and the electrons are then transferred to the CNTs. This process retards the recombination of the electron–hole pairs in the photocatalytic system. However, the electrons transferred to the CNTs cannot be used effectively in photocatalytic reactions, since CNT surfaces are not only chemically inert but also catalytically inactive. The catalytic activity of TiO_2 photocatalysts has been improved previously by the addition of particles of metals such as Pt [20]. The

* Corresponding author. Tel.: +81 92 802 2752; fax: +81 92 802 2752.
E-mail address: takenaka@chem-eng.kyushu-u.ac.jp (S. Takenaka).

0926-3373/$ – see front matter © 2012 Elsevier B.V. All rights reserved.
http://dx.doi.org/10.1016/j.apcatb.2012.06.013

electrons generated in Pt-added TiO_2 under UV light irradiation are transferred to the Pt particles and the adsorbed species on the Pt metal are then reduced by the electrons; an example of this process is water splitting, where the reduction of protons forms hydrogen molecules. Thus, the catalytic activity of the TiO_2–CNT composites as photocatalysts should be improved by the deposition of Pt metal particles in the composites.

In the present work, we demonstrated that CNTs could be uniformly covered with TiO_2 nanoparticles, using the hydrolysis and condensation of titanium tetraisopropoxide ($Ti(O^iPr)_4$) in the presence of urea or glycine amide. The urea or glycine amide added during the hydrolysis of $Ti(O^iPr)_4$ acted as linker molecules between the TiO_2 nanoparticles and the CNT surface, which led to the uniform coverage of CNT surfaces with TiO_2 nanoparticles. In addition, Pt metal particles were deposited in the CNT cavity of the TiO_2–CNT composites. These composite catalysts showed excellent photocatalytic activity for the photodegradation of organic molecules in water.

2. Experimental

2.1. Coverage of CNT with TiO_2 nanoparticles

The CNTs (multi-walled CNTs) were washed with aqueous HCl (3.6 M) at 353 K to remove metal impurities. The CNTs thus obtained were refluxed in concentrated HNO_3 solution (68 wt%) at 395 K for 14 h to introduce oxygen-containing functional groups such as hydroxyl and carboxylic groups on the CNT surfaces. The CNTs were thoroughly washed with distilled water and dried in air at 353 K.

$Ti(O^iPr)_4$ was diluted with 2-propanol and aqueous HCl (3.6 mol L^{-1}) was then added to the solution. The CNTs were ultrasonically dispersed in this solution at room temperature. Urea was added and the solution was heated to 323 K in air under magnetic stirring. The concentration of urea in this solution was adjusted to 33 mmol L^{-1}. After filtration, the samples thus obtained were dried at 333 K in air and were calcined at 603 K in air. Thermogravimetric analysis of the TiO_2–CNT composites in air showed that the CNTs in the composites were gradually gasified at temperatures higher than 650 K.

2.2. Characterization of the catalysts

The morphology of the TiO_2–CNT composites was observed using transmission electron microscopy (TEM; JEOL-2000EX). The TiO_2–CNT composites were dispersed in 2-propanol, using ultrasonic irradiation at room temperature. Some of this solution was dropped onto a TEM grid and was dried at 333 K.

X-ray diffraction (XRD) patterns were measured for the TiO_2–CNT composites using a Rigaku RINT2000 (Cu Kα = 1.5141 Å).

Fourier transform IR (FT-IR) spectra were taken for the TiO_2 samples using a JASCO FT/IR-4200. The TiO_2 sample was pressed into a thin pellet after being mixed with KBr.

2.3. Photodegradation of organic molecules in water, using the TiO_2–CNT composites

The photocatalytic degradation of acetic acid was performed over the TiO_2-based catalysts in a conventional batch-typed reactor made from quartz. The catalyst was loaded in the reactor such that the amount of TiO_2 was the same (0.010 g) for all of the reactions. The catalyst was dispersed and stirred in an aqueous solution of acetic acid (0.2 mol L^{-1}) for 3 h at room temperature under an oxygen atmosphere in the dark. The suspension was irradiated using an ultra-high pressure Hg lamp (500 W) at room temperature. During the reaction, some of the gases in the reaction apparatus were sampled and were analyzed using a gas chromatograph with a thermal conductivity detector. The photocatalytic degradation of other organic molecules was performed over the catalysts using a similar method to that used for the photodegradation of acetic acid.

3. Results and discussion

3.1. Preparation of TiO_2–CNT composites

The CNTs were dispersed in a mixed solution of $Ti(O^iPr)_4$, 2-propanol and aqueous HCl to prepare the TiO_2–CNT composites without any linker molecules. The obtained composite will hereafter be referred to as TiO_2–CNT(none). Fig. 1(a) and (b) shows TEM images of the TiO_2–CNT(none) composite. The loading of TiO_2 in the composites was determined to be 45 wt% using thermogravimetric analysis in air. CNTs were observed in the TEM images; the diameter of the CNTs ranged from 15 to 30 nm. Many particles were deposited on the outer surfaces of the CNTs. As described below, these particles observable in the TEM images were assignable to TiO_2 in anatase phase, as determined from the XRD patterns of the corresponding sample. Many TiO_2 particles were deposited on the outer surfaces of the CNTs in the TiO_2–CNT(none) composite, but exposed CNT surfaces were also frequently observed in these TEM images. In addition, many TiO_2 particles that were not in contact with any CNT surface were observed in the TEM images of the composites. During the preparation of TiO_2–CNT(none), the hydrolysis and condensation of $Ti(O^iPr)_4$ proceeded to form TiO_2 nanoparticles. In the present study, CNTs were treated with concentrated HNO_3 to introduce oxygen-containing functional groups on the CNT surfaces, which acted as anchoring sites for the TiO_2 nanoparticles. The interaction between the TiO_2 nanoparticles and the functional groups on the CNT surfaces was not so strong that the whole CNT surface could be covered with TiO_2 particles. It is likely that the density of the functional groups on the CNT surfaces was not high enough to ensure uniform coverage with TiO_2 nanoparticles.

The preparation of TiO_2–CNT composites was performed using the hydrolysis of $Ti(O^iPr)_4$ in the presence of urea. The CNTs were dispersed in a mixed solution of $Ti(O^iPr)_4$, 2-propanopl and aqueous HCl, and urea was then added to the solution. The composite thus obtained will hereafter be referred to as TiO_2–CNT(urea). TEM images of the TiO_2–CNT(urea) composite are shown in Fig. 1(c) and (d). The TiO_2 loading in the composite was evaluated to be 58 wt%. The entire surface of the CNTs in the TiO_2–CNT(urea) sample seemed to be uniformly covered with TiO_2 nanoparticles, suggesting that the urea added during the hydrolysis of $Ti(O^iPr)_4$ acted as linker molecules between the CNTs and the TiO_2 nanoparticles. The TiO_2–CNT(urea) sample was calcined in air at 1073 K to clarify the coverage of CNTs with TiO_2 nanoparticles. CNTs in the TiO_2–CNT(urea) sample were removed by gasification with oxygen during the calcination in air at 1073 K. Fig. 1(e) and (f) shows TEM images of the TiO_2–CNT(urea) composite after calcination in air. The fibrous TiO_2 observable in these TEM images seemed to have inner cavities. We therefore concluded that the CNTs could be uniformly covered with TiO_2 nanoparticles using the hydrolysis and condensation of $Ti(O^iPr)_4$ in the presence of urea.

The thickness of the TiO_2 particle layers wrapped around the CNTs could be controlled by changing the $Ti(O^iPr)_4$ concentration during the preparation of TiO_2–CNT(urea). Fig. 2 shows TEM images of TiO_2–CNT(urea) prepared at $Ti(O^iPr)_4$ concentrations of 8.5 and 34 mmol L^{-1}, while the TiO_2–CNT(urea) samples shown in Fig. 1 were prepared using a $Ti(O^iPr)_4$ concentration of 17 mmol L^{-1}. The CNTs were uniformly covered with TiO_2 nanoparticles in all TiO_2–CNT(urea) samples. It was noted that the outer diameter of the TiO_2–CNT(urea) composites became larger with higher $Ti(O^iPr)_4$ concentrations. The TiO_2 loading in the

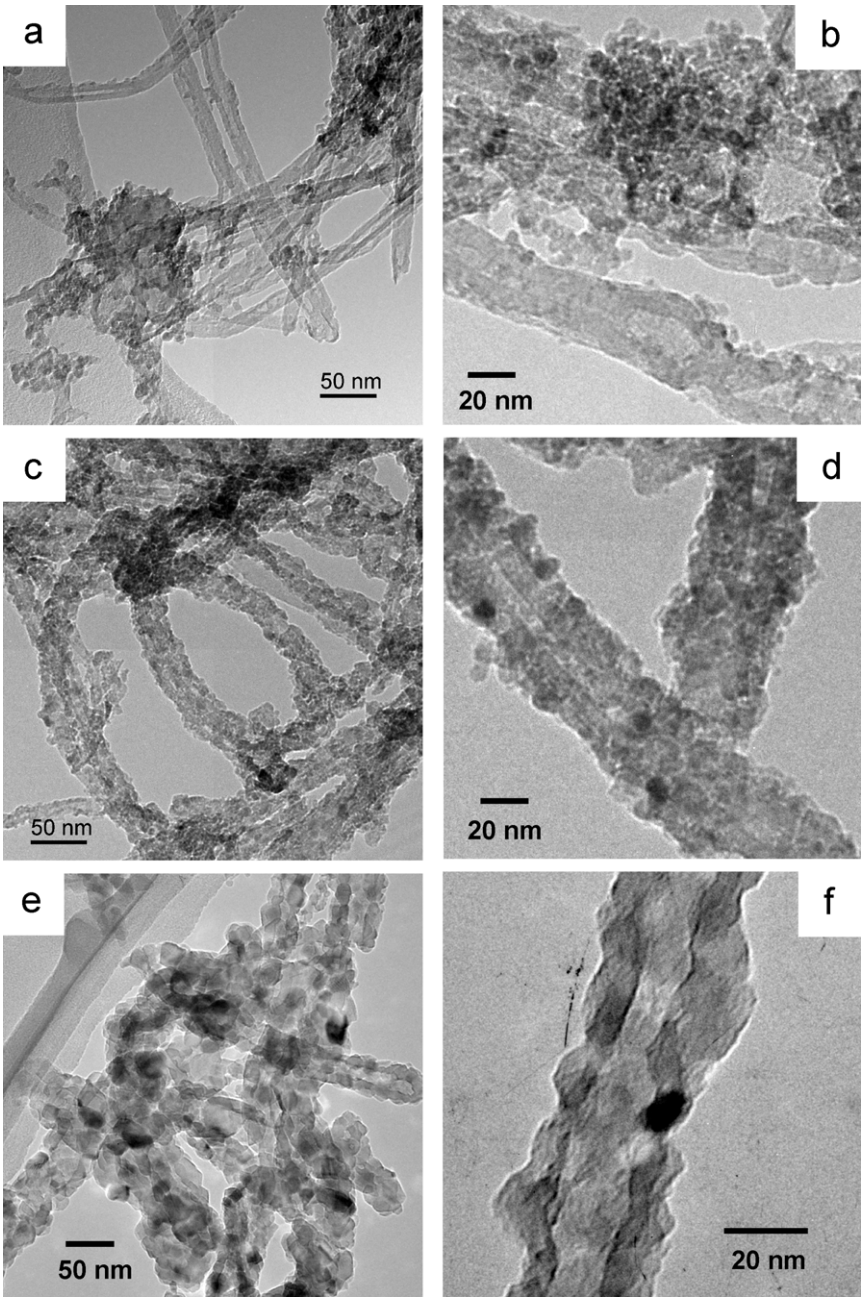

Fig. 1. TEM images of TiO_2–CNT composites. TiO_2–CNT(none) (a and b), TiO_2–CNT(urea) (c and d) and TiO_2–CNT(urea) calcined in air at 1073 K (e and f).

TiO_2–CNT(urea) samples prepared at $Ti(O^iPr)_4$ concentrations of 8.5, 17 and 34 mmol L^{-1} was estimated to be 42, 58 and 73 wt%, respectively. The thickness of the TiO_2 particle layers deposited on the CNT surfaces could thus be controlled by changing the concentration of $Ti(O^iPr)_4$.

Fig. 3 shows XRD patterns for TiO_2–CNT(none) and TiO_2–CNT(urea) samples prepared at different concentrations of $Ti(O^iPr)_4$. The XRD pattern for the TiO_2–CNT(urea) sample before calcination at 603 K in air is also shown in Fig. 3. The strong peak observed at $2\theta = 26^\circ$ in the XRD patterns for all the samples was assignable to the (0 0 2) graphitic basal plane reflection of CNTs. In the XRD pattern for TiO_2–CNT(urea) before calcination, no strong diffraction peaks except for the peak due to CNT could be found, implying that the TiO_2 structure was amorphous. In contrast, diffraction lines corresponding to TiO_2 in an anatase phase were found in the XRD patterns for all of the TiO_2–CNT composites after calcination at 603 K. Based on the XRD patterns shown in Fig. 3, the average TiO_2 crystallite size in the TiO_2–CNT composites was evaluated using Scherrer's equation. The average anatase TiO_2 crystallite size in the TiO_2–CNT(urea) samples prepared at $Ti(O^iPr)_4$ concentrations of 8.5, 17 and 34 mmol L^{-1} was estimated to be 5.9, 6.4 and 6.7 nm, respectively. The average TiO_2 crystallite size in TiO_2–CNT(none) prepared at a $Ti(O^iPr)_4$ concentration of 17 mmol L^{-1} was estimated to be 5.7 nm, which was slightly smaller than that determined for TiO_2–CNT(urea). The addition of urea during the hydrolysis of $Ti(O^iPr)_4$ would lead to an increase in the TiO_2 crystallite size.

3.2. Role of urea in the TiO_2-coating

As described earlier, the outer surface of the CNTs was uniformly covered with TiO_2 nanoparticles using the hydrolysis of

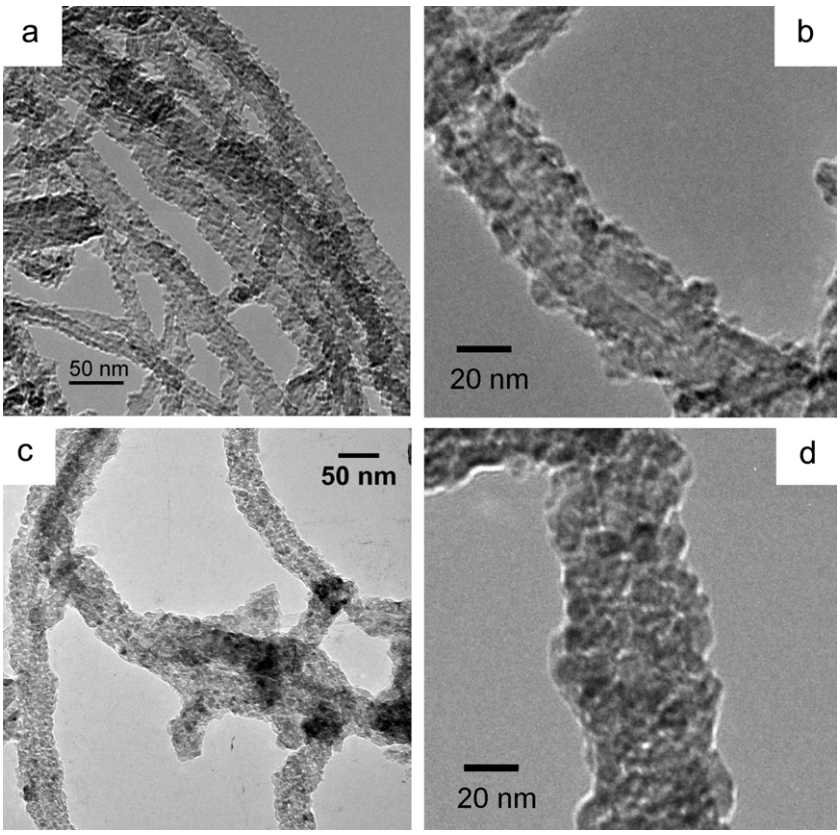

Fig. 2. TEM images of TiO_2–CNT(urea) prepared at $Ti(O^iPr)_4$ concentrations of 8.5 mmol L^{-1} (a and b) and 34 mmol L^{-1} (c and d).

$Ti(O^iPr)_4$ in the presence of urea, while exposed CNT surfaces were frequently observed in the TiO_2–CNT composites prepared in the absence of urea. The urea added during the hydrolysis of $Ti(O^iPr)_4$ acted as a linker molecule to enhance the interaction between the TiO_2 nanoparticles and the CNTs. The FT-IR spectrum of the TiO_2 nanoparticles was measured. After the hydrolysis of $Ti(O^iPr)_4$ in the presence of urea, the TiO_2 obtained was washed with distilled water and dried at 353 K in air. Fig. 4 shows the FT-IR spectrum of the obtained TiO_2. Bands were observed at approximately 1650, 1565 and 1490 cm^{-1}. This spectrum was consistent with that of urea species adsorbed on Fe_2O_3–TiO_2 catalysts [21]. The urea species coordinated on the catalyst surface with an N atom from an amine group and an O atom from a carbonyl group, while another amine group in the adsorbed urea did not interact with the catalyst surface. During the hydrolysis of $Ti(O^iPr)_4$ in the presence of urea, the free amine group in the urea adsorbed on TiO_2 nanoparticles should interact with the CNT surfaces, leading to the uniform coverage of the CNTs with TiO_2 nanoparticles. We have already reported the uniform coverage of CNTs with thin silica layers via the hydrolysis of 3-aminopropyltriethoxysilane (APTES) [22,23]. During the preparation of silica-coated CNT, amine groups in APTES strongly

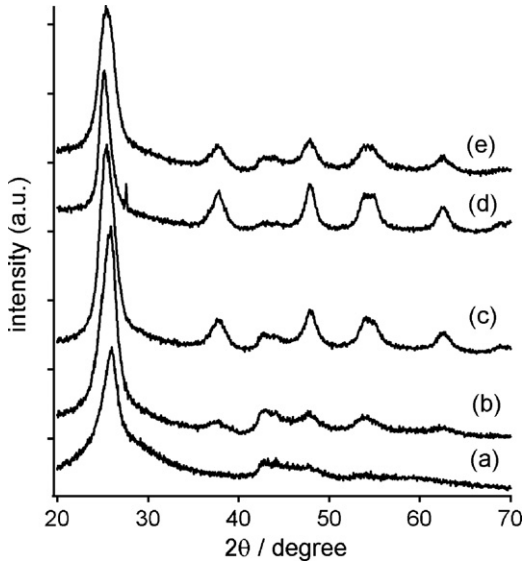

Fig. 3. XRD patterns of TiO_2–CNT composites. (a) Uncalcined TiO_2–CNT(urea) prepared at a $Ti(O^iPr)_4$ concentration of 17 mmol L^{-1}; (b–d) calcined TiO_2–CNT(urea) prepared at $Ti(O^iPr)_4$ concentrations of 8.5, 17 and 34 mmol L^{-1}, respectively; (e) calcined TiO_2–CNT(none) prepared at a $Ti(O^iPr)_4$ concentration of 17 mmol L^{-1}.

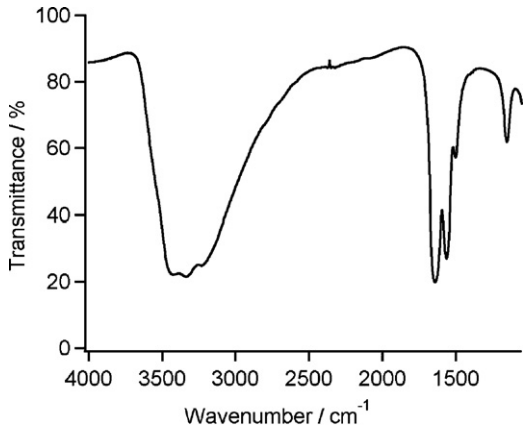

Fig. 4. FT-IR spectrum of TiO_2 prepared using the hydrolysis of $Ti(O^iPr)_4$ in the presence of urea.

interacted with graphene and/or carboxylic groups on the CNTs to form uniform silica layers. Thus, the presence of the urea linker molecules during the hydrolysis of $Ti(O^iPr)_4$ resulted in the uniform coverage of the CNTs with TiO_2 nanoparticles.

To further clarify the role of urea in the coverage of the CNTs with TiO_2 nanoparticles, the hydrolysis and condensation of $Ti(O^iPr)_4$ were performed in the presence of acetamide (CH_3CONH_2), oxamide ($(CONH_2)_2$), methylurea ($NH_2CONH(CH_3)$), ethylenediamine ($NH_2CH_2CH_2NH_2$), 3-amino-1-propanol (NH_2-$CH_2CH_2CH_2OH$) or glycine amide ($NH_2CH_2CONH_2$). The concentration of these molecules was adjusted to a similar value (33 mmol L^{-1}) to that of urea. Fig. 5 shows TEM images of the TiO_2–CNT composites prepared in the presence of these molecules. The TiO_2 loading in these TiO_2–CNT composites ranged from 60 to 70 wt%. In the TEM images of the TiO_2–CNT composites prepared in the presence of acetamide (panel a), oxamide (panel b) and methylurea (panel c), exposed CNT surfaces and aggregated TiO_2 particles were frequently observed, although some CNT surfaces were covered with TiO_2 nanoparticles. This is due to the absence of amino groups in acetamide, methylurea, or oxamide (which would have interacted with the CNT surfaces), although these molecules adsorb on TiO_2 particles through —$CONH_2$ groups. Aggregated TiO_2 particles and exposed CNT surfaces were also frequently observed in the TEM images of the TiO_2–CNT composites prepared in the presence of ethylenediamine (panel d) or 3-amino-1-pronanol (panel e). Ethylenediamine and 3-amino-1-pronanol have amine groups to allow interactions with the CNTs, but they have no —$CONH_2$ groups to allow interactions with the TiO_2 nanoparticles. Thus, the CNT surfaces were not uniformly covered with TiO_2 nanoparticles after the hydrolysis of $Ti(O^iPr)_4$ in the presence of acetamide, oxamide, methylurea, ethylenediamine, or 3-amino-1-propanol. In contrast, TiO_2 nanoparticles were uniformly and densely deposited on the CNT surfaces and exposed CNT surfaces were seldom found in the TiO_2–CNT composites prepared in the presence of glycine

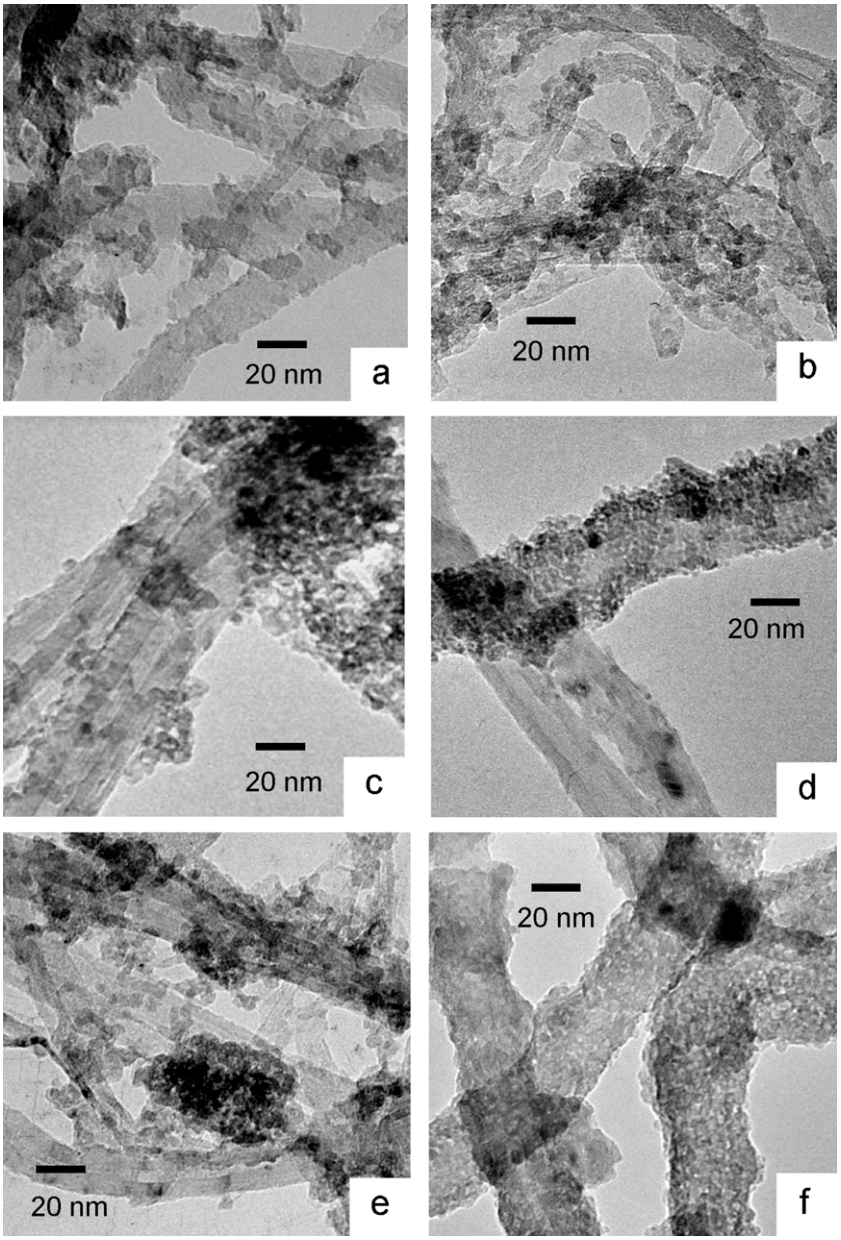

Fig. 5. TEM images of TiO_2–CNT composites prepared by the hydrolysis of $Ti(O^iPr)_4$ in the presence of acetamide (a), oxamide (b), methylurea (c), ethylenediamine (d), 3-amino-1-propanol (e), or glycine amide (f).

amide. This coverage of the CNTs with TiO_2 nanoparticles could be achieved via the hydrolysis of $Ti(O^iPr)_4$ in the presence of glycine amide because the $-CONH_2$ in the glycine amide adsorbed on the TiO_2 nanoparticles and another amine group in the glycine amide that was adsorbed on the TiO_2 was in contact with the CNT surfaces. The CNTs were thus uniformly covered with TiO_2 nanoparticles using the hydrolysis of $Ti(O^iPr)_4$ in the presence of urea or glycine amide. These linker molecules are easily removed by calcination of the catalysts in air, as compared to surfactant molecules such as sodium dodecylsulfate, which have been frequently utilized for the coverage of CNTs with TiO_2. It is reported that the addition of urea during the preparation of TiO_2 does not spoil the photocatalytic activity of TiO_2 thus obtained [24]. Thus, our method is effective for the modification of CNT surfaces with metal oxides.

3.3. Coverage of CNT@Pt with TiO_2 nanoparticles

TiO_2 photocatalysts are frequently deposited on CNT surfaces to retard the recombination of photogenerated hole–electron pairs in TiO_2 [6,7]. Electrons photogenerated in the TiO_2–CNT composites travel into the CNTs. However, the photogenerated electrons on the CNTs cannot be utilized efficiently for photocatalytic reactions, because the graphene surface generally shows poor activity for catalytic reactions. The TiO_2–CNT(urea) samples were therefore modified with Pt metal particles in the present study. When Pt metal particles were deposited in the CNT cavity of the TiO_2–CNT(urea), the electrons photogenerated in the TiO_2 traveled to the Pt metal through the CNTs and the electrons on the Pt metal participated in catalytic reactions. The reaction involving the photogenerated holes occurred on the TiO_2 particles in the TiO_2–CNT(urea) composites with Pt metal. The active Pt and TiO_2 sites in the composite catalysts would therefore have a low susceptibility for facilitating the backward reaction of the process in applications such as the recombination of H_2 and O_2 in water splitting systems.

Fig. 6 shows the CNT-supported Pt metal particles. The CNT-supported Pt metal particles were prepared via the incipient wetness method, using aqueous H_2PtCl_6 [25]. The Pt loading in the catalysts was estimated to be 6.0 wt% by thermogravimetric analysis in air. In TEM images of the CNT-supported Pt catalysts, Pt metal particles were observed and their diameter ranged from 1 to 3 nm. Most of the Pt metal particles seemed to be deposited in the cavity of CNTs (see TEM image (a)). To further clarify the position of the Pt metal particles in the Pt catalysts, TEM images were taken after the samples were tilted from −30° to 30°. The TEM images for the Pt catalysts are also shown in Fig. 6. The Pt metal particles in the CNT-supported Pt catalysts were seldom found on the outer surfaces of the CNTs but they were observed in the center of the CNTs as the tilting angle of the sample was changed. If the Pt metal particles were present on the outer surfaces of CNTs, they could be observed in the TEM images on the outer surfaces or graphene layers of the CNTs, as the tilting angle of the samples was changed. These results indicated that the Pt metal particles in the CNT-supported Pt metal catalysts were mainly stabilized in the cavities of the CNTs. The CNTs had open ends and their surface property was hydrophilic, since the CNTs had been treated with concentrated HNO_3 before the deposition of Pt metal. Thus, an aqueous H_2PtCl_6 solution was sucked into the CNTs by the capillary actions during the impregnation and then Pt metal particles were formed in the cavities of CNTs during the treatment with hydrogen. Thus, many Pt metal particles were stabilized in the cavities of CNTs. Hereafter, the CNT-supported Pt metal catalyst will be referred to as CNT@Pt.

The CNT@Pt composite was covered with TiO_2 nanoparticles via the hydrolysis of $Ti(O^iPr)_4$ in the presence of urea. The composite

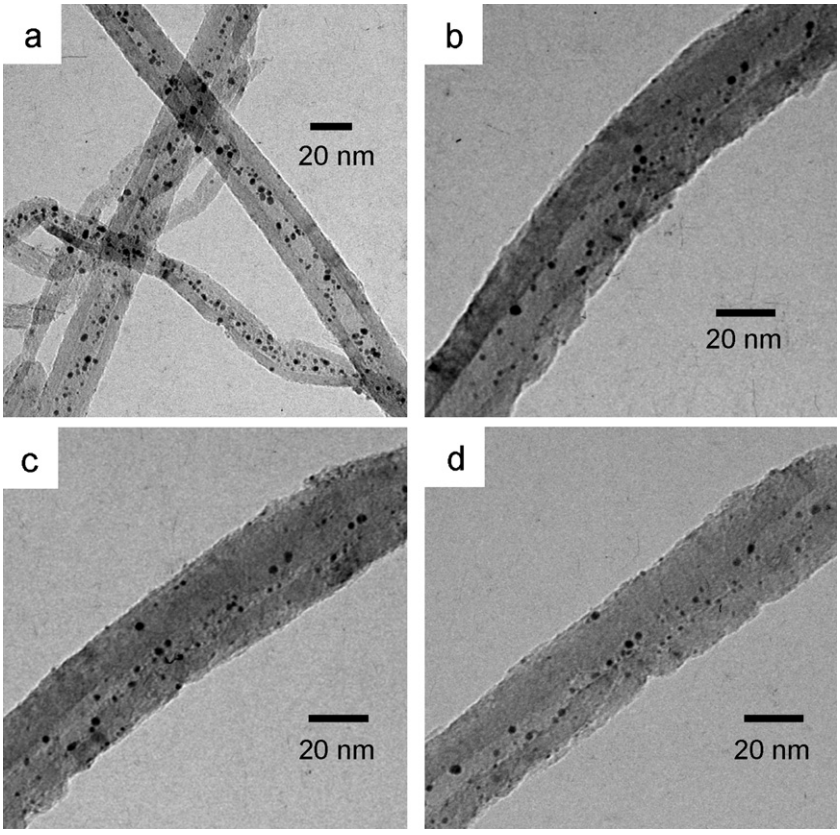

Fig. 6. TEM images of CNT@Pt catalysts. (b), (c) and (d) were measured at a sample tilting angle of −30°, 0° and +30°, respectively.

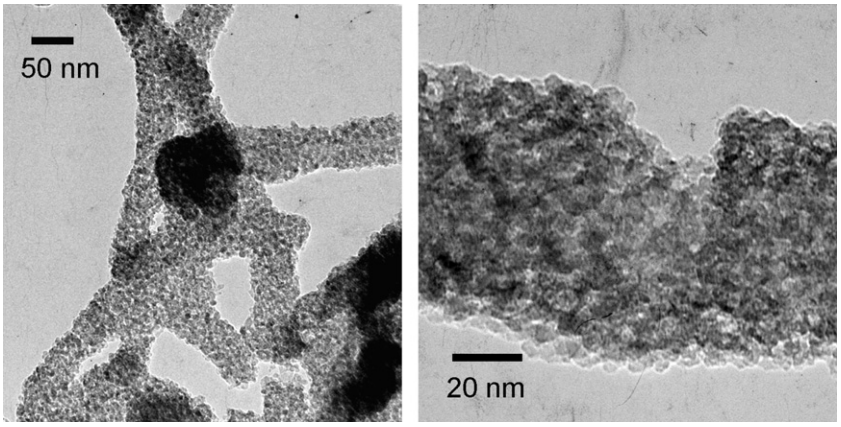

Fig. 7. TEM images of TiO_2–CNT@Pt(urea).

thus obtained was denoted as TiO_2–CNT@Pt(urea). TEM images of the TiO_2–CNT@Pt(urea) composite are shown in Fig. 7. The outer surface of CNT@Pt could be uniformly covered with TiO_2 nanoparticles via the hydrolysis of $Ti(O^iPr)_4$ in the presence of urea. The Pt and TiO_2 loading in the TiO_2–CNT@Pt(urea) composite was evaluated to be 1.5 and 76 wt%, respectively.

3.4. Photocatalytic activity of TiO_2–CNT composites

The photodegradation of acetic acid was performed over different TiO_2–CNT composites to clarify their catalytic activity. TiO_2–CNT(urea) with TiO_2 loading = 73 wt% and TiO_2–CNT(none) with TiO_2 loading = 65 wt% were used as photocatalysts. The TiO_2 powders (which were prepared via the hydrolysis of $Ti(O^iPr)_4$ in the presence of urea followed by calcination at 603 K in air) were mixed with CNTs simply by using a mortar. The TiO_2 loading in the physical TiO_2–CNT mixture was adjusted to be 73 wt%. For comparison, TiO_2 powder (P25, Degussa) was also used as the catalyst. Fig. 8 shows the photoirradiation time-dependent changes in the amount of CO_2 formed during the photodegradation of acetic acid over TiO_2-based catalysts (performed at room temperature). For all of the reactions over all of the catalysts, CO_2 was the main gas formed, with small amounts of methane also being formed. The amount of CO_2 formed increased linearly with photoirradiation time for all reactions over all of the catalysts. TiO_2 prepared in this study showed a similar activity to TiO_2 (P25) for the photodegradation of acetic acid. The addition of CNTs to the TiO_2 photocatalytic system increased the catalytic activity. The catalytic activity of TiO_2–CNT(urea) was higher than that of both a mixture of TiO_2 and CNT, and TiO_2–CNT(none). The intimate interaction between the TiO_2 and the CNTs enhanced the transition of the photogenerated electrons from the TiO_2 to the CNTs during the photocatalytic reactions.

The photodegradation of acetic acid was performed repeatedly over the TiO_2–CNT(urea) catalysts in order to clarify the durability of the catalysts. Fig. 9 shows the change of catalytic activity of TiO_2–CNT(urea) in the repeated photodegradation of acetic acid. After the photodegradation of acetic acid, the TiO_2–CNT(urea) was recovered by filtration and then the recovered catalyst was dispersed again in an aqueous solution of acetic acid. Catalytic activity of TiO_2–CNT(urea) in each run normalized by its activity in the first run is shown in Fig. 9. The catalytic activity of TiO_2–CNT(urea) was gradually decreased as the photocatalytic reactions were repeated. However, the decrease in the catalytic activity of TiO_2–CNT(urea) was quite small. The TiO_2–CNT(urea) showed high durability for the photodegradation of acetic acid.

Fig. 10 shows the change in the amount of CO_2 formed during the photodegradation of acetic acid over TiO_2–CNT(urea) and TiO_2–CNT@Pt(urea). For comparison, Pt metal particles were deposited on TiO_2–CNT(urea) via the impregnation of

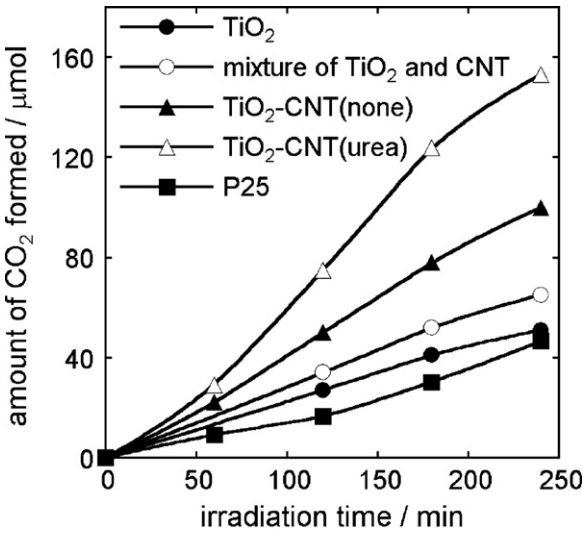

Fig. 8. Changes in the amount of CO_2 formed during the photodegradation of acetic acid over TiO_2-based catalysts.

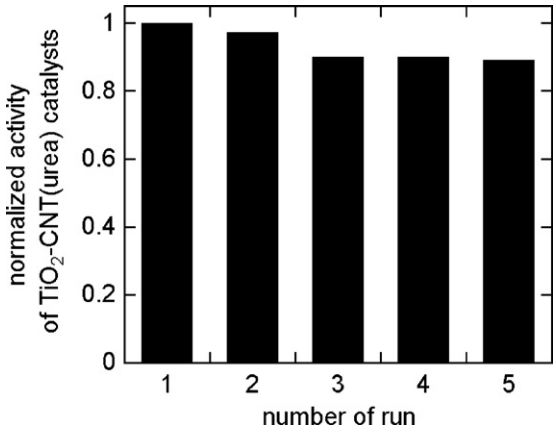

Fig. 9. Changes in the catalytic activity of TiO_2–CNT(urea) for the repeated photodegradation of acetic acid.

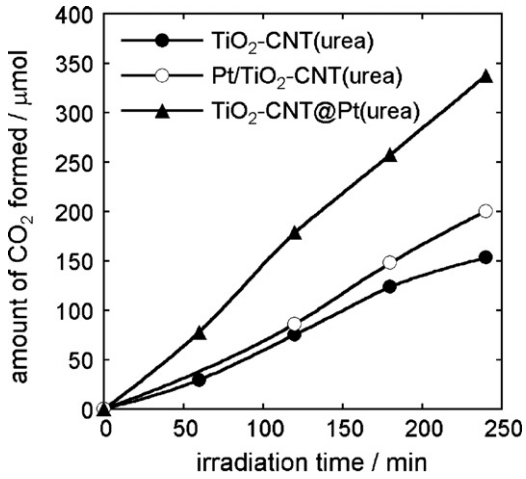

Fig. 10. Changes in the amount of CO_2 formed during the photodegradation of acetic acid over TiO_2-based catalysts.

TiO_2–CNT(urea) into an aqueous solution of H_2PtCl_6, followed by reduction with hydrogen at 473 K. The Pt and TiO_2 loading in the composites was estimated to be 1.9 and 72 wt%, respectively. The Pt catalysts supported on TiO_2–CNT(urea) were denoted as Pt/TiO_2–CNT(urea). The Pt metal particles in Pt/TiO_2–CNT(urea) were mainly deposited on the TiO_2 nanoparticles that were wrapped around the outer surfaces of CNTs, while most of Pt metal particles in TiO_2–CNT@Pt(urea) were stabilized in the cavities of the CNTs. The photocatalytic activity of TiO_2–CNT(urea) was further enhanced by the addition of the Pt metal particles. TiO_2–CNT@Pt(urea) showed the higher catalytic activity for the photodegradation of acetic acid than Pt/TiO_2–CNT(urea). The Pt metal in the composites provided catalytically active sites. Oxygen molecules adsorbed on the Pt metal were activated by the photogenerated electrons in the TiO_2–CNT@Pt(urea) to form active oxygen species for the degradation of acetic acid. The deposition of Pt metal particles in the cavities of the CNTs in TiO_2–CNT(urea) prevented backward reactions because the photogenerated electrons on the Pt metal were separated from the holes on the TiO_2 in the TiO_2–CNT@Pt(urea) catalysts. Thus, TiO_2–CNT@Pt(urea) showed higher catalytic activity for the photodegradation of acetic acid than Pt/TiO_2–CNT(urea).

The photodegradation of methanal, propanal, butanal and hexanal was carried out over TiO_2–CNT@Pt(urea) and Pt/TiO_2–CNT(urea) to clarify their catalytic performance. In the photocatalytic degradation of all of the substrates tested in the present study, CO_2 was the main gas formed, in addition to small amounts of hydrogen and methane. The amount of CO_2 formed increased linearly with the photoirradiation time for the reactions of all of the substrates over both of the catalysts; this was similar to the results shown in Figs. 8 and 10. The formation rates of CO_2 are shown in Fig. 11(a) for the reactions of each substrate. The catalytic activity of TiO_2–CNT@Pt(urea) for the photodegradation of methanal was significantly higher than that of Pt/TiO_2–CNT(urea). In contrast, Pt/TiO_2–CNT(urea) showed higher catalytic activity for the photodegradation of butanal and hexanal compared with TiO_2–CNT@Pt(urea). To clarify the differences between the catalytic performances of the two composite catalysts, the relative activity of the TiO_2–CNT@Pt(urea) substrate—compared with the activity of the Pt/TiO_2–CNT(urea) substrate—is shown in Fig. 11(b). Interestingly, the activity of TiO_2–CNT@Pt(urea) gradually decreased relative to that of Pt/TiO_2–CNT(urea) as the size of substrate molecules became larger. These results implied that larger molecules were oxidized with more difficulty over the Pt catalysts in the CNT cavities of TiO_2–CNT@Pt(urea). The substrates would have been oxidized by the photogenerated holes on the TiO_2, or by hydroxyl radicals formed by holes and water molecules. In addition, the substrates were oxidized by active oxygen species formed from photogenerated electrons and molecular oxygen. In the reactions over TiO_2–CNT@Pt(urea), the substrates were oxidized on the Pt metal particles in the cavities of the CNTs, as well as on the TiO_2 nanoparticles wrapped around the CNTs. The larger substrates diffused to the Pt metal in the CNT cavities with more difficulty. Thus, the relative activity of TiO_2–CNT@Pt(urea) (compared with that of Pt/TiO_2–CNT(urea)) decreased as the size of the substrates became larger. These results suggested that the selectivity in the catalytic reactions could be controlled based on the size of substrate molecules using the TiO_2–CNT@Pt(urea) photocatalysts.

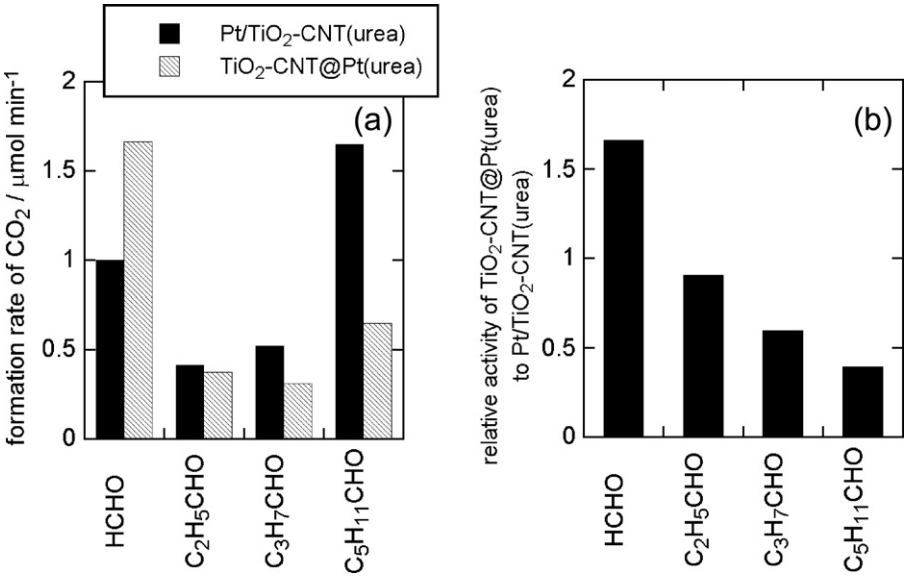

Fig. 11. Photodegradation of various substrates over TiO_2–CNT@Pt(urea) and Pt/TiO_2–CNT(urea) catalysts. (a) Formation rate of CO_2 for the photodegradation of each substrate and (b) relative activity of TiO_2–CNT@Pt(urea) to Pt/TiO_2–CNT(urea) for the photodegradation of each substrate.

4. Conclusions

The outer surfaces of CNTs could be uniformly covered with TiO_2 nanoparticles using the hydrolysis of $Ti(O^iPr)_4$ in the presence of urea and glycine amide. Urea and glycine amide acted as linker molecules between the TiO_2 nanoparticles and the CNTs. The TiO_2–CNT(urea) composites showed higher catalytic activity for the photodegradation of organic impurities in water than TiO_2 alone, or a physical mixture of TiO_2 and CNTs. The intimate interaction between the TiO_2 and CNTs resulted in the facile transition of photogenerated electrons from the TiO_2 to the CNTs, which retarded the recombination of electron–hole pairs. The stabilization of Pt metal particles in the cavities of CNTs in the TiO_2–CNT(urea) composite further improved its photocatalytic activity.

Acknowledgments

The present work was supported by a Grant-in-Aid of Scientific Research (B) (No. 23360359) from the Ministry of Education, Culture, Science, Sports and Technology of Japan.

References

[1] D. Eder, Chemical Reviews 110 (2010) 1348–1385.
[2] A. Bianco, K. Kostarelos, M. Prato, Chemical Communications 47 (2011) 10182–10188.
[3] J.T. Sun, C.Y. Hong, C.Y. Pan, Polymer Chemistry 2 (2011) 998–1007.
[4] S.H. Lee, D.H. Lee, W.J. Lee, S.O. Kim, Advanced Functional Materials 21 (2011) 1338–1354.
[5] X. Pan, X. Bao, Accounts of Chemical Research 44 (2011) 553–562.
[6] K. Woan, G. Pyrgiotakis, W. Sigmund, Advanced Materials 21 (2009) 2233–2239.
[7] R. Leary, A. Westwood, Carbon 49 (2011) 741–772.
[8] C. Aprile, A. Corma, H. Garcia, Physical Chemistry Chemical Physics 10 (2008) 769–783.
[9] U.G. Akpan, B.H. Hameed, Applied Catalysis A: General 375 (2010) 1–11.
[10] Y. Paz, Applied Catalysis B: Environmental 99 (2010) 448–460.
[11] A. Jitianu, T. Cacciaguerra, R. Benoit, S. Delpeux, F. Béguin, S. Bonnamy, Carbon 42 (2004) 1147–1151.
[12] W. Wang, P. Serp, P. Kalck, J.L. Faria, Applied Catalysis B: Environmental 56 (2005) 305–312.
[13] S. Wang, L. Ji, B. Wu, Q. Gong, Y. Zhu, J. Liang, Applied Surface Science 255 (2008) 3263–3266.
[14] X. Yan, B.K. Tay, Y. Yang, Journal of Physical Chemistry B 110 (2006) 25844–25849.
[15] F.F. Cao, Y.G. Guo, S.F. Zheng, X.L. Wu, L.Y. Jiang, R.R. Bi, L.J. Wan, J. Maier, Chemistry of Materials 22 (2010) 1908–1914.
[16] J. Sun, M. Iwasa, L. Gao, Q. Zhang, Carbon 42 (2004) 895–899.
[17] S. Lee, W.M. Sigmond, Chemical Communications (2003) 780–781.
[18] W. Fan, L. Gao, J. Sun, Journal of the American Ceramic Society 89 (2006) 731–733.
[19] B. Gao, C. Peng, G.Z. Chen, G.L. Puma, Applied Catalysis B: Environmental 85 (2004) 17–23.
[20] A. Kudo, Y. Miseki, Chemical Society Reviews 38 (2009) 253–278.
[21] M.A. Larrubia, G. Ramis, G. Busca, Applied Catalysis B: Environmental 30 (2001) 101–110.
[22] S. Takenaka, H. Matsumori, K. Nakagawa, H. Matsune, E. Tanabe, M. Kishida, Journal of Physical Chemistry C 111 (2007) 15133–15136.
[23] S. Takenaka, T. Arike, H. Matsune, E. Tanabe, M. Kishida, Journal of Catalysis 257 (2008) 345–355.
[24] P. Cheng, C. Deng, M. Gu, X. Dai, Materials Chemistry and Physics 107 (2008) 77–81.
[25] X. Pan, Z. Fan, W. Chen, Y. Ding, H. Luo, X. Bao, Nature Materials 6 (2007) 507–511.